ICARUS 105, 216–224 (1993)

# Target Porosity Effects in Impact Cratering and Collisional Disruption

STANLEY G. LOVE

*Department of Astronomy, FM-20, University of Washington, Seattle, Washington 98195*

FRIEDRICH HÖRZ

*Geology and Geophysics Branch, NASA Johnson Space Center, Houston, Texas 77058*

AND

DONALD E. BROWNLEE

*Department of Astronomy, FM-20, University of Washington, Seattle, Washington 98195*

Received April 7, 1993; revised June 14, 1993

**We present the results of a series of eight experimental hypervelocity impacts of soda lime glass projectiles into porous sintered aggregate glass targets with varying strengths and densities. Increased target porosity leads to deeper crater penetration, lower spall velocities, and greater localization of the impact damage. Rear surface spallation is also greatly reduced in porous targets. Estimates of the specific energy required to destroy targets of varying porosity indicates that this threshold is proportional to (1-porosity)$^{-3.6}$, much greater than the dependence on unconfined compressive strength, and implying that the lifetimes of porous meteoroids and interplanetary dust particles against collisional disruption are longer than previously predicted. These experiments also produced melt-lined agglutinate crater pits, often well preserved despite total disruption of the target.** 

## 1. INTRODUCTION

The collisional destruction and comminution of finite-sized objects is the subject of ongoing experimental and theoretical studies aimed at a better understanding of the evolution of asteroids and the interplanetary meteoroid population. Although much effort focuses on the extension of small-scale laboratory results to larger sizes where gravity plays an important role (e.g., Fujiwara *et al.* 1989, Housen *et al.* 1991), the experimental results should be directly applicable to the destruction of meteoroids and interplanetary dust particles (Grün *et al.* 1985). Nevertheless, the space exposure times inferred from the measured abundances of $^{26}$Al and $^{10}$Be in ~400-$\mu$m diameter cosmic spherules (Nishiizumi *et al.* 1991) are as much as two orders of magnitude greater than the collisional lifetimes predicted on the basis of the laboratory impact results. This discrepancy could be attributed to differences in the physical properties of the experimental targets and natural meteoroids. In particular, target porosity may play a substantial role.

Porous targets are known to be poor transmitters of impact shock because their component solids and void spaces present extreme acoustic impedance mismatches. The multiple shock reverberations occurring at grain boundaries effectively dissipate a disproportionately large amount of energy into highly localized volume fractions of the target (e.g., Kieffer 1971, Ahrens and Cole 1974, Cintala 1992) as compared to the dense, homogeneous materials typically employed in the aforementioned experiments. In porous media, the projectile's kinetic energy is partitioned more effectively into target heating and into spallation, disruption, and crushing of the component grains to fill the void spaces. Porous targets, therefore, should suffer less displaced material in cratering events and show an increased resistance to collisional fragmentation. On the other hand, natural materials with high porosity often exhibit poor cohesion and generally decreased compressive yield strength. The latter effect leads to the expectation of increased displaced crater volume per unit incident kinetic energy (e.g., Holsapple and Schmidt 1987) and *decreased* resistance to impact disruption.

Because the role of compressive strength has been the subject of numerous studies (e.g., Fujiwara *et al.* 1989, Housen *et al.* 1991), the objective of the present study was to explore specifically the effect of porosity on collisional



0019-1035/93 $5.00

disruption. Ideally, any experimental variable of interest should be isolated by tests that employ otherwise identical conditions. This ideal is not, however, readily achieved with target porosity, because of the apparent impracticality of manufacturing targets of widely differing porosity at constant compressive strength. Instead, we produced targets of known and highly variable porosity by sintering glass beads under differing conditions and used their measured compressive strengths to separate out the effect of porosity. Our target ensemble also included objects of constant porosity but variable strength, to provide a check on the assumed strength effects. The targets were subjected to two sets of projectiles resulting either in crater-forming events or in complete collisional disruption of the entire target. The total number of trials conducted in the experiment was fairly modest because the effort was perceived to be a preliminary study to establish possible directions for more extensive future efforts.

## 2. EXPERIMENTAL PROCEDURES

### *2.1. Target Manufacture and Properties*

In order to produce consistent and well-characterized porous target blocks, we sintered soda lime glass beads of 50 $\mu$m diameter and 2.5 g cm$^{-3}$ nominal density (bulk-purchased Ballotini impact beads from Potter Industries, Canby, OR). A sintering process was chosen in order to make a loosely bonded solid aggregate material analogous to porous natural meteoroids. The small bead size was chosen so that the grain-scale inhomogeneities in the target would be much smaller than the projectile. Cylindrical holes, 7.5 cm in diameter by 3.8 cm deep, were drilled in large blocks of graphite to serve as molds. The molds were filled to the top with glass beads, using repeated gentle tapping as the only method of compressing the charge. For each set of three identical targets, the filled molds were heated together in an oven for 240 min, after which the oven was switched off. The long baking time was chosen to help facilitate uniform heating in the molds and their contents. The oven's bulk thermal inertia and insulation resulted in a gradual cooling of its contents to room temperature over a period of several hours, and the oven was not opened until the following day. The long cooling time was employed in order to minimize possible internal thermal stresses in the targets. Varying the oven temperature between 643 and 695°C with constant baking times resulted in coherent, sintered target blocks with reproducible porosities and strengths. The target properties are summarized in Table I. Of the three identical targets produced in each heating run, one was used for mechanical strength testing and the second and third subjected to "cratering" and "collisional fragmentation" experiments, respectively.

TABLE I
Target Properties

| Target Type | Sintering Temp. (C) | Density (g/cc) | Porosity (%) | Strength (kbar) |
|---|---|---|---|---|
| A | 643 | 1.50 | 39 | 0.079 |
| B | 658 | 1.58 | 37 | 0.44 |
| C | 695 | 2.44 | 5 | 2.8 |
| D | 672 | 1.00 | 60 | 0.020 |

The Types A and B targets were intended to have similar densities, but different strengths. Their porosities were close to 36%, the theoretical value for an ensemble of close-packed spheres. These targets were white in color, and their constituent beads were still identifiable. The Type C targets were dark, opaque, and glassy; the beads initially comprising them had lost their individual identities. The Type D targets, with 60% porosity, were manufactured by mixing the customary solid beads in a 1 : 1 volume ratio with hollow glass microballoons which served as fillers. The resulting targets shed parts of themselves with even the gentlest handling. In a separate test, a sample of unmixed microballoons was heated under similar conditions but showed no sign of self-cohesion or sintering. We are therefore confident that the target strength is controlled by the sintered portions of the solid beads and that the added microballoons changed the bulk porosity of these targets, but not their other material properties. We are likewise confident that the three examples of each target type were identical to one another, as we assured thermal equilibrium during sintering as well as possible.

It is also important to know whether the bulk material properties are homogeneous within each target block. This was checked by sawing an initial test specimen in half, and testing for physical inhomogeneity by scratching different parts of the sawn face with a sharp tool. The result of this test was that the targets were at least qualitatively homogeneous.

### *2.2. Strength Testing*

One copy of each target type was reserved for unconfined compressive strength testing at the University of Washington's Materials Science and Engineering Laboratory. Cylindrical cores, 2.5–4 cm in height and 2.3 cm in diameter, were drilled from the center of each target, with their axes parallel to that of the cylindrical target. The cores were placed in an Instron 4505 load frame, which provided records of the force applied and the displacement of the moving crosshead. The unconfined compressive strength values thus obtained are presented in Table I.

TABLE II
Projectile Parameters

| JSC Shot # | Target Type | Diameter (mm) | Mass (g) | Velocity (km/s) | Energy (erg) |
|---|---|---|---|---|---|
| 1088 | C | 1.588 | 0.00568 | 6.013 | 1.03E+09 |
| 1089 | A | 1.588 | 0.00554 | 5.965 | 9.85E+08 |
| 1090 | B | 1.588 | 0.00539 | 6.056 | 9.88E+08 |
| 1091 | D | 1.588 | 0.00556 | 6.0 * | 1.00E+09 |
| 1092 | C | 3.175 | 0.03745 | 5.353 | 5.37E+09 |
| 1093 | B | 3.175 | 0.03724 | 4.868 | 4.41E+09 |
| 1094 | D | 3.175 | 0.03731 | 5.483 | 5.61E+09 |
| 1095 | A | 3.175 | 0.03754 | 4.851 | 4.42E+09 |

* No velocity measurement available, but consistent with preceding three shots.

Samples of Types A, B, and D targets showed well-determined breaking points. Despite their weak cohesion and tendency to compress, they all broke decisively, usually along a diagonal plane from the center of one end to a point on the edge of the other. Their strength values were based on testing of a single sample. The Type C sample, strongest and most brittle of all, did not behave as well, so the measurement was repeated twice more. In two of the three cases, small shape irregularities caused the outer layers of the cylinder to spall completely off, leaving thin cores of indeterminate area supporting the measured load. Only one broke decisively, yielding a strength value near the center of the factor of ~5 variance between the others. We use the result of the final trial as the best estimate of the material's strength.

### 2.3. *Impact Experiments and Definitions*

The impact experiments were carried out at the light gas gun facility at NASA Johnson Space Center (JSC). For each of the four different target types, two experiments were conducted, as summarized in Table II: one using a 1/16-inch (1.6-mm) soda lime glass projectile at a nominal velocity of 6 km $sec^{-1}$ to investigate cratering and rear surface spallation, and another using a 1/8-inch (3.2-mm) glass projectile at a nominal 5 km $sec^{-1}$ to address collisional disruption at higher specific energies.

Each target was mounted in a sealed plexiglass target box, measuring 30 × 30 × 60 cm, with a removable lid and a 1.5-cm-diameter entrance hole for the projectile. The details of the target mounting changed for the different shots.

In the low-energy shots (JSC numbers 1088–1091) the target was securely clamped in place between a plastic backplate and an open front face ring that grabbed the edges of the target. The backplate in turn was affixed to the massive rear ("downrange") wall of the collection box. Beginning with experiment 1089, an inked 1100 alloy aluminum witness plate, 3.2 mm thick and equipped with a suitable entrance hole for the projectile, monitored the crater ejecta at the "uprange" end of the box. These shots also featured thin (75 $\mu$m) aluminum foil sleeves wrapped around the target to form cylindrical witness plates. The foil sleeves served the dual purpose of recording fast, low-angle ejecta from the uprange side of the target and providing extra assurance that material spalled from the back and sides of the target would not mix with the uprange crater ejecta. The spallation fragments from shot 1088 remained trapped in the mounting clamp, allowing them to be collected separately from the crater ejecta despite the lack of a foil sleeve.

The collisional fragmentation shots at higher specific energy (1092–1095) required that the targets be suspended in a way that minimized shock reflections and other undesirable edge effects caused by the mounting itself. To accomplish this, the targets were fastened in loops of thin copper wire attached to positioning rods that protruded from the massive rear wall of the collection box. A piece of foam rubber was positioned between the target and the backplate to cushion the downrange fragments. With the target mounted in this way, it was impossible to separate the uprange and downrange material. An imperfect attempt to collect ejecta was made by placing the uprange witness plate 30 cm closer to the target. The fragments that successfully cleared the hole in the witness plate to be trapped in the space between it and the front wall of the collection box are certainly part of the uprange "ejecta," but comprise only an indeterminate fraction thereof.

Each target was sanded flat prior to being measured for precise dimensions and weight. The target and collection box were assembled and placed into the impact chamber of a 5-mm-diameter light gas gun, fired at chamber pressures of 1–2 × $10^{-3}$ torr. After firing, the entire box was removed from the impact chamber and carefully disassembled. The materials in the forward and aft compartments were collected separately. The largest remaining fragment—variously the cratered but substantially intact target of the cratering shots or the relatively small fragments produced by the high-energy shots—was termed the "core." All of the material caught behind the foil sleeve or pinned between the core and the backplate in the low-energy shots was termed "spall," in contrast to the crater "ejecta" in the uprange space. The terms spall and ejecta as used in this report refer to the location of their recovery, and are not intended to imply detailed knowledge of how they were formed: processes besides spallation could contribute to the aft compartment material, and the crater ejecta includes material spalled from the target's front face near the impact site. In the high-

TABLE III
Shot Results

| JSC Shot # | Target Type | Target Mass (g) | Specific Energy (erg/g) | Core Mass (g) | Ejecta Mass (g) | Spall Mass (g) | Debris Mass (g) | Mass Lost (g) |
|---|---|---|---|---|---|---|---|---|
| 1088 | C | 246.0 | 4.19E+06 | 227.21 | 2.12 | 16.67 | 18.79 | (b) |
| 1089 | A | 256.10 | 3.85E+06 | 253.65 | 2.32 | 0.13 | 2.45 | (b) |
| 1090 | B | 276.61 | 3.57E+06 | 275.03 | 1.28 | 0.30 | 1.58 | (b) |
| 1091 | D | 113.33 | 8.80E+06 | 112.26 | 0.80 | 0.27 | 1.07 | (b) |
| 1092 | C | 254.51 | 2.11E+07 | 14.92 | 2.11 | (a) | 235.53 | 1.95 |
| 1093 | B | 278.04 | 1.59E+07 | 200.48 | 0.15 | (a) | 76.63 | 0.78 |
| 1094 | D | 115.73 | 4.85E+07 | 17.87 | 0.0 | (a) | 69.45 | 1.41 |
| 1095 | A | 265.74 | 1.66E+07 | 5.64 | 1.36 | (a) | 256.80 | 2.16 |

(a) Not applicable for these shots.
(b) Not measured.

energy shots, all of the material in the downrange compartment was termed "debris." Recovery, even at high energies, was better than 99% of the original target mass. Most of the missing mass probably escaped through the projectile entrance hole in the target box. The various fragment masses for each experiment are summarized in Table III.

## 3. RESULTS

### *3.1. Cratering Experiments*

The low-energy shots produced prominent craters, so completely dominated by front surface spall zones that the central, symmetric crater "pit" could not be established with confidence. The craters appeared as rough, shallow depressions akin to those described by others for laboratory cratering events in solid, brittle targets (e.g., Gault 1973, Polanskey and Ahrens 1990). An example is illustrated in Fig. 1.

Porosity seems to have some effect on the morphology of these spall zones, as suggested by measurements of their maximum and minimum diameters and their depths, all of which are presented in Table IV. The least porous target yielded the shallowest crater, and the most porous one is penetrated the deepest. This seems in keeping with the findings of Hörz *et al.* (1993) who reported on the relationship between penetration depth and target density or porosity. In Fig. 2, we compare the present findings with the summary of Hörz *et al.* (1993). The new data points show scatter on a scale comparable to those of previous experiments, but are systematically offset toward relatively deeper penetrations, an effect for which we have no good explanation. None of the craters are glass lined, and indeed (as detailed below) the glass lined pits have been removed from the impact sites. Thus, mass removal below the craters' melt zones must have taken place, most likely by spallation. The depths we measured may therefore not be directly analogous to those reported by Gault (1973) for dense $SiO_2$ glass or to those of Hörz *et al.* (1993) for the much deeper penetration tracks in extremely porous media, which exhibit no spallation at

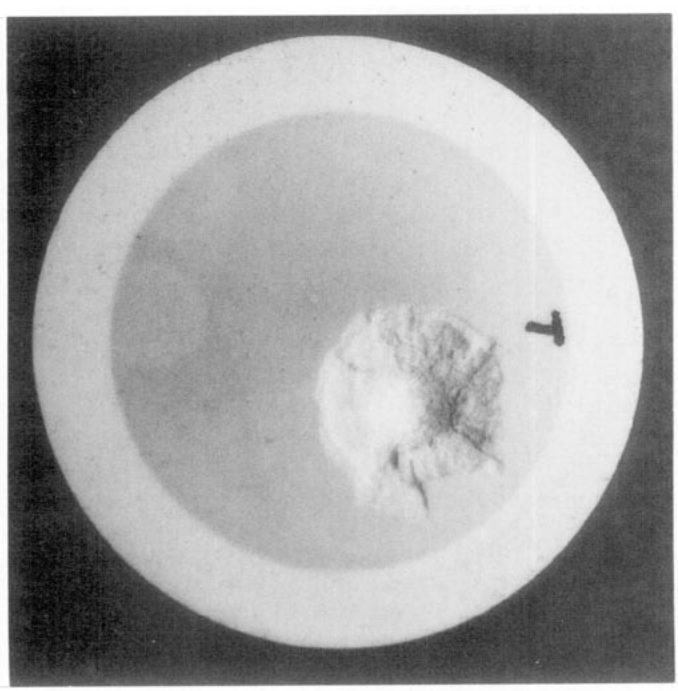

FIG. 1. A photograph of the target of experiment 1090, showing the impact crater spallation zone.

TABLE IV
Crater Measurements

| JSC Shot # | Target Type | Max. Diam. (mm) | Min. Diam. (mm) | Ave. Diam. (mm) | Depth (mm) | Depth/Diameter Ratio |
|---|---|---|---|---|---|---|
| 1091 | D | 20 | 13 | 16 | 9 | 0.56 |
| 1089 * | A | 40 | 27 | 34 | 9 | 0.26 |
| 1090 | B | 28 | 25 | 26 | 8 | 0.31 |
| 1088 | C | 28 | 25 | 26 | 5 | 0.19 |

* Projectile landed near edge of target, producing unnaturally large spall zone.

the bottom of the central crater. Additionally, no attempt has been made to compensate for differences in target properties (such as compressive strength) which might contribute to the vertical scatter of the plotted points.

As listed in Table III, the total ejecta mass depends on the target type. If the result of shot 1089 is neglected because of its off-center impact point and associated increased spallation from edge effects, the ejecta mass is observed to vary systematically with target density, strength, or porosity, although with the present data it is not possible to determine which of those parameters is most responsible for the trend. The mass–density relationship suggests that ejecta *volume* is roughly constant, regardless of the strength or porosity. Consideration of strength alone suggests that more mass is displaced with the same impact energy in the stronger but denser targets, a seemingly nonsensical result for craters of a size that should be totally dominated by strength-related effects (Gault 1973, Holsapple and Schmidt 1987). On the other hand, the trend with porosity suggests that the hypothesized poor shock transmission properties of porous materials lead to less excavated mass at constant strength. The observed constant ejecta volume is probably a fortuitous circumstance resulting from a tradeoff between strength effects and the increasingly rapid spatial decay of shock stresses with higher porosity.

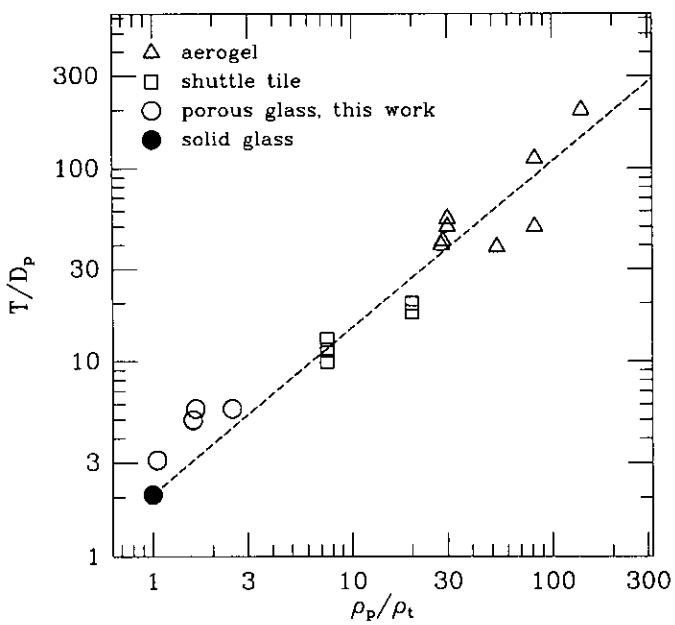


FIG. 2. Penetration depth ($T$) over projectile diameter ($D_p$) as a function of projectile-to-target density ratio for light gas gun shots at ~6 km/sec into a variety of porous silicates, with no attempt made to compensate for other target properties. The shuttle tile points (squares) are adapted from Christiansen and Ortega (1990), while the aerogel points (triangles) are from Hörz *et al.* (1993), and the solid glass point (filled circle) is from Gault (1973). The current results (hollow circles) are consistently above the best-fit line of the others, but do not show appreciably more scatter.

Some qualitative inferences about the velocity of the ejecta fragments may be drawn from the aluminum witness plates. Fast-moving ejecta should readily penetrate the foil sleeves or produce secondary crater damage on the more massive front plates. Only two experiments, 1088 and 1092, which employed the dense, strong Type C targets, showed any damage on the massive plates, in the form of minor dents and penetrations of the ink layer. The aluminum sleeve of shot 1091 recorded nothing, but those of experiments 1089 and 1090 intercepted a thin sheet of fine-grained ejecta emerging with a half-cone angle of ~60°. Again, all damage was confined to the ink layer, and there was no perforation of the thin foil. The porous and weak targets seemingly could not support the large stress amplitudes, characteristic of more dense and competent targets, that are required to accelerate materials to high velocities. While no quantitative velocities can be established for the observed ejecta, they seem to be consistent with the results of Nakamura and Fujiwara (1991), who report velocities of less than 50 m sec$^{-1}$ for the majority of fragments emanating from similar experiments using dense basalt and alumina targets.

### *3.2. Backside Spallation*

Given the thickness of our targets, the low-energy shots were devised to produce a full-fledged crater in the front

of the target, while permitting possible spallation of the rear surfaces to occur if their behavior were similar to the dense rocks employed in the cratering experiments of Gault (1973) and the collisional fragmentation study of Cintala and Hörz (1984). These latter experiments were also used as guides to assure collisional disruption of the entire target in the higher specific energy experiments.

Not surprisingly, the expectations for rear surface spallation were met only by the type C targets, the nearest equivalent to the nonporous, competent targets in the background experiments discussed above. Shot 1088 displaced almost an order of magnitude more mass at the rear surface than in the impact crater. While minute quantities of material were recovered in the spall compartment in the other three low-energy experiments, there was only negligible rear-wall spallation. The origin of the recovered materials, all very fine-grained, often could not be traced to discernable damage on the target's rear face; we suspect that it may have been dislodged from the target during its mounting and handling, or that it is actually some finely divided ejecta that may have made it into the rear compartment through the joints between the target and forward clamp ring. Whatever the origin of the material, the pronounced lack of backside spallation phenomena in all targets possessing substantial porosity once again attests to the poor transmission of shock energy through highly porous targets. This generalization holds even for materials with such poor strength and cohesion that they were difficult to handle manually without damaging them.

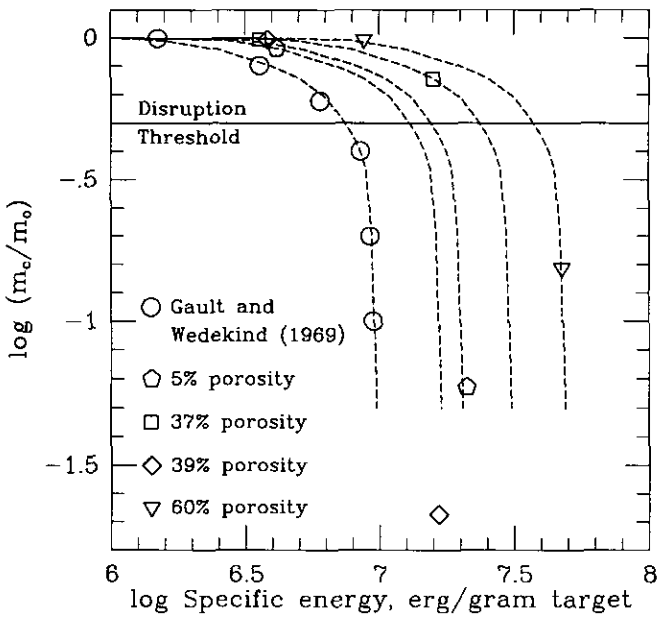


FIG. 3. Log of core-to-original mass ratio, plotted as a function of impactor kinetic energy per unit mass. The data of Gault and Wedekind (1969) are shown, as is the 50% mass reduction line defining collisional disruption. The dotted curves are fits to the Gault and Wedekind points, shifted horizontally to best match the points for each kind of target in this study, giving us an estimate of their disruption energies.

### *3.3. Collisional Disruption*

The high specific energy experiments were designed to study complete impact disruption of the targets. Here we adopt conventional terminology and definitions to describe the collisional events and their products: a target is deemed "destroyed" if the remaining core mass ($m_c$) constitutes less than half the initial target mass ($m_0$). The specific energy (ergs of projectile kinetic energy per gram initial target mass) for the condition that $m_c = 0.5\ m_0$ is the "threshold" energy for collisional disruption. We also consider the largest target fragment, even if its mass is much less than $0.5\ m_0$, remaining after collisions at specific energies higher than the aforementioned threshold value to be a valuable indicator for the degree of collisional disruption (e.g., Fujiwara *et al.* 1989, Rubin *et al.* 1991).

The masses of the target cores and largest core fragments for our four target types are plotted in Fig. 3, which also illustrates an attempt to reconstruct their disruption threshold energies via a number of model assumptions. The latter lean heavily on the experiments by Gault and Wedekind (1969) employing glass spheres, which we deem the closest available analogues to our target materials. The Gault and Wedekind curve describes the specific energy dependence of the largest target fragment mass through the front-plus-rear spallation and complete disruption regimes. By horizontal translation of this curve so that it passes through each of our data points we obtain, at least in principle, an intersection with the horizontal disruption threshold line at $m_c = 0.5\ m_0$ for each target type. We are aware that direct modeling of our experimental results with the Gault and Wedekind data neglects a number of known factors; for these reasons, we deem the procedure fairly qualitative, but justifiable in order to obtain an intercomparison of our targets and some measure of their relative behavior. Of prime import is the fact that experiments of this type are fraught with large scatter in the data and that measurement of a single fragment from a single shot may not necessarily characterize any target with great accuracy (Rubin *et al.* 1991). Also, a number of studies have revealed differences in the behavior of cubical and spherical targets, suggesting that the geometrical shape of finite-sized targets affects collision outcomes. We used cylinders, unlike the spheres of Gault and Wedekind (1969). Additionally, we include the results of the cratering shots, which may not be exactly analogous to the lowest-energy experiments of Gault and Wedekind, although it should be pointed out that our low-energy shots have only a very minor effect on the final location of the translated curve. Finally, a number of studies point out that the exact shape of such collisional disruption curves

depends on target strength as well (e.g., Davis and Ryan 1990). While comparison with the Gault and Wedekind (1969) experiments is deemed most appropriate and justified for our least porous target, we recognize that application of this curve to targets of different rheology is highly model-dependent. As a consequence, specific values obtained for disruption threshold energies based on this procedure must be viewed with considerable caution and may not be viewed as established experimental results. We will proceed with these model results, nevertheless, to develop some sense of relative behavior and general trends.

The disruption energies extrapolated from Fig. 3 are listed in Table V for more convenient evaluation of their dependency on porosity and compressive strength. The Types A and B targets had nearly identical porosities but different unconfined compressive strengths. Hörz *et al.* (1975, but see also Gault *et al.* 1972, and Gault 1973) derived a general formula for disruptive events, specifically including the compressive strength term, $S$, measured in kbar,

$$E_d/m = 4.6 \times 10^6 S^{0.45} r^{-0.225},$$

where $E_d/m$ is the disruption threshold energy (erg g$^{-1}$) and $r$ is the target radius (cm). The strength ratio between the Types A and B targets is 5.6; the above equation therefore predicts disruption energies that differ by a factor of 2.2, which compares closely with our value of 1.8. Thus, our (only) two data points at constant porosity but different strength seem consistent with the strength dependency of that relation. The Type C targets, densest of all, should be the closest analogue to the targets employed by Gault (1973). It therefore seems reasonable to assume that our densest and more competent material will comply with the $S^{0.45}$ trend as well. Making the (admittedly substantial) assumption that the Type D targets also conform to the $S^{0.45}$ dependence, we may use our measured compressive strengths to isolate and solve for the functional dependence of porosity alone. In Fig. 4 we plot the observed $E_d/m$ divided by $S^{0.45}$ as a function of the solid fraction of the target (1 − porous fraction); consideration of the solid fraction only avoids mathematical problems at zero porosity for logarithmic plots. Our four data points form a surprisingly straight line in view of all the uncertainties involved. That line yields:

$$E_d/m = 7.57 \times 10^6 S^{0.45} (1 - \text{porosity})^{-3.6}.$$

While we do not ignore that this analysis is based on a small number of experiments and that it contains substantial model assumptions, we nevertheless obtain an exponent on porosity that appears very large, indeed quite beyond expectation, and certainly significantly larger than any exponent on target strength. We must conclude that target porosity affects collisional outcomes to a much larger extent than compressive strength. Porous targets are simply very poor transmitters of shock waves and capable of consuming most of an impacting projectile's kinetic energy in a region close to the impact point.

TABLE V
Disruption Energies

| Target Type | Porosity (%) | Strength (kbar) | Disruption Energy (erg/g) |
|---|---|---|---|
| A | 39 | 0.079 | 1.3E+07 |
| B | 37 | 0.44 | 2.4E+07 |
| C | 5 | 2.8 | 1.6E+07 |
| D | 60 | 0.020 | 3.8E+07 |

### 3.4. Impact Melts

While the production of impact melt in porous targets made of materials with relatively low melting points was not unexpected at these impact velocities (e.g., Stöffler *et al.* 1975, Cintala 1991), the unusual habit and shape of some of the melt products of this study need mentioning. The only target where melt was found lining the crater bottom was that of experiment 1088, the low-energy shot against the least porous target type. All other targets spalled sufficiently to quantitatively dislodge all melts.

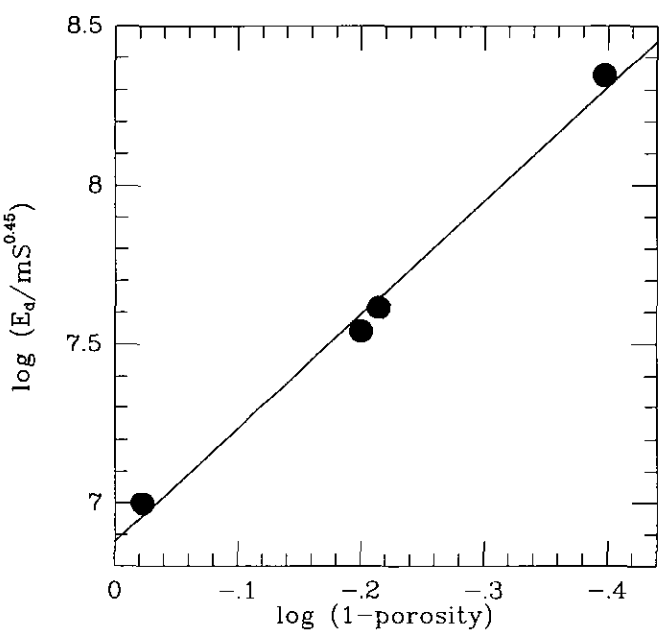


FIG. 4. The effect of porosity on disruption energy, with the effect of unconfined compressional strength compensated for using the $S^{0.45}$ rule. The surprisingly good best-fit line has a slope of −3.6.

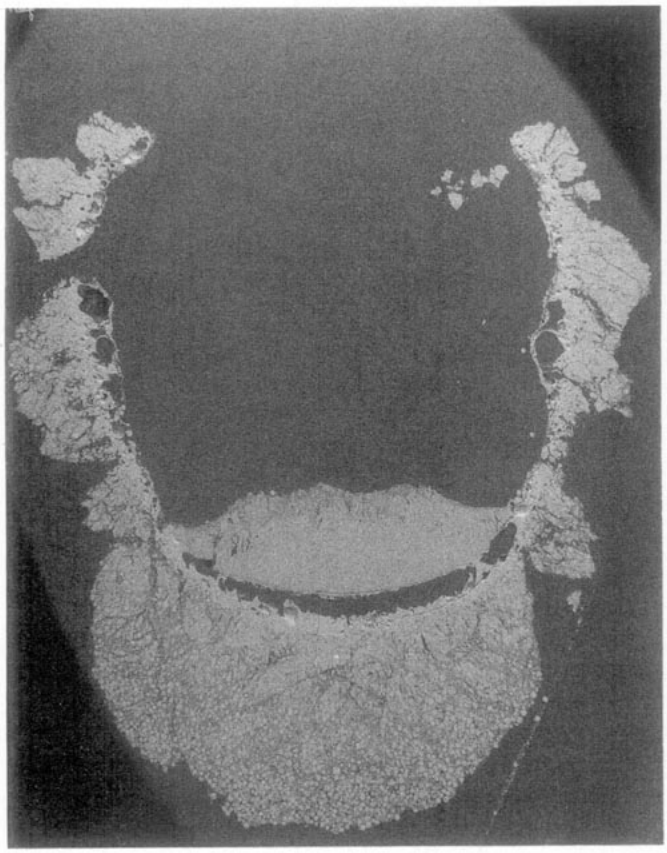

FIG. 5. Photograph of a section of the intact, detached glass-lined pit produced in experiment 1095. The target was completely disrupted. The mass at the crater bottom is the substantially intact but deformed projectile.

The 39 and 37% porosity (Types A and B, respectively) targets produced and displaced unusually well-preserved glass objects that represent entire glass-lined pits or substantial fragments thereof. A sectioned sample of such a glass-lined pit is illustrated in Fig. 5, showing a roughly hemispherical shell of totally melted and optically transparent material on the interior surfaces, with highly fractured and crushed target material on the exterior. Similar "melt-liners" were recovered not only from the intended cratering experiments, but also from targets that were totally disrupted. The case shown in Fig. 5 had a largest fragment of only 0.02 × the original target mass. The result here is that intact melt-liners may survive fairly energetic events that collisionally annihilate the parent object. Also, unusually rapid cooling rates are suggested for these melts to quench into shapes that preserve a growing crater cavity which evolves in a matter of milliseconds.

These melt objects have morphological equivalents in some unusually well preserved, albeit rare, lunar agglutinates (McKay *et al.* 1991). The preservation of doughnut-shaped lunar agglutinates or substantial fragments thereof in the form of arcuate shapes that resemble broken crater "rims" lead some to conclude that only one agglutinate is produced in each lunar regolith impact, and that, therefore, the size-frequency distribution of agglutinates should reflect that of the associated micrometeorite impactors (e.g., Lindsay 1975). While our experimentally produced melt-liners are unusually good morphological analogues to these (rare) lunar melt particles, our experiments demonstrate that Lindsay's postulate was incorrect, as already suggested by many others (e.g., McKay *et al.* 1991). Most lunar samples for which any case for a melt-lined pit could be made with confidence are fragments. Entire intact specimens are rarities. Note the complex geometry of the experimental specimen and envision the difficulties in reconstructing the size of the original pit from any single, arbitrary fragment. Further, our experiments produced melt-liners and additional, irregular melt particles which demonstrate that a multitude of glassy objects of various shapes will result from individual impacts into porous targets, contrary to Lindsay (1975).

Preservation of these delicate specimens, even in totally disruptive events, is surprising. Furthermore, the fact that they were not comminuted during secondary collisions with the walls of collection box or the witness plates and other obstacles within it mandates exceptionally low takeoff speeds. These experimental glass melt-liners, therefore, once again raise the general question of the fate and whereabouts of potential asteroidal agglutinates which have been searched for, but not found, in meteorites that resemble regolith breccias (e.g., summary by Hörz and Schaal 1981.) The lack of agglutinates in these meteorites is commonly explained with the assumption that most or all molten impact products will have ejection speeds greater than the escape velocities of their parent objects. This assumption needs reevaluation.

## 4. SUMMARY AND CONCLUSION

In summary, our small series of hypervelocity light gas gun shots against specially prepared targets with known and different porosities has produced a number of results that attest to the poor shock transmission of materials with substantial porosity. In the low specific energy cratering events, increasing porosity led to greater penetration depths, generally consistent with the trend reported by Hörz *et al.* (1993). Despite their lower unconfined compressive strengths, the porous targets suffered roughly the same excavated crater volumes as the denser, more competent ones. Only the least porous of our target types was able to support stress amplitude high enough to accelerate spallation fragments to velocities sufficient to mark a massive witness plate; ejecta from the others was probably released at speeds below 50 m $sec^{-1}$. Similarly, the densest target suffered extensive rear-surface spallation at a specific energy that produced only insignificant liberation of material in the more porous bodies.

By modeling our targets using the results of Gault and Wedekind (1969) for impact destruction of glass spheres, we were able to find semiquantitative values for our targets' disruption threshold energies. Comparing the two targets with the same porosity but different unconfined compressive strength yielded results consistent with the $S^{0.45}$ dependence of the disruption threshold reported by Gault (1973). By assuming that this relation holds for the other target types, we were able to estimate that the disruption threshold scales with $(1 - \text{porosity})^{-3.6}$. This exponent was unexpectedly large, in particular much greater than the exponent of the strength term. Despite the large uncertainties in the derivation of this exponent, we conclude that porosity is more important than strength in determining the outcome of disruptive impacts. Despite the strong porosity effect that we found, it is probably sufficient to increase the collisional lifetimes of meteoroids with reasonable compressive strengths (Wasson 1974) and moderate porosities by a factor of only ~2 over the predictions of the Grün *et al.* (1985) model, insufficient to resolve the discrepancy between their observed space exposure ages and their predicted collisional lifetimes. It is clear that much more experimental and theoretical work is needed in this area before reliable, quantitative treatment of the collisional lifetimes of porous meteoroids becomes possible.

Finally, these experiments produced melt-lined crater pits, similar to rare agglutinate specimens found in the lunar soil (McKay *et al.*, 1991), that often appeared to be completely intact, even when the parent object was utterly destroyed. Their survival requires that their takeoff velocities were exceptionally low, a finding that challenges the assumption that all melt products formed in asteroidal regoliths have speeds sufficient to escape their parent objects.

## ACKNOWLEDGMENTS

The authors thank Gerald Haynes, Frank Cardenas, and William Davidson for their excellent operation of the light gas gun facility at JSC. We would also like to thank Bob Morley, the University of Washington Physics Shop glassblower, for the use of his oven in making the targets and for cutting the strength test core samples at the expense of personal bodily injury. We also acknowledge the help of Mark Richards of U. W. Materials Science and Engineering for conducting the target strength tests. This work was supported by NASA.

## REFERENCES

AHRENS, T. J., AND D. M. COLE 1974. Shock compression and adiabatic release of lunar fines from Apollo 17. *Proc. Lunar Sci. Conf., 5th,* 2333–2345.

CHRISTIANSEN, E. L., AND J. ORTEGA 1990. *Hypervelocity Impact Testing of Shuttle Orbiter Thermal Protection System Tiles.* AIAA Space Programs and Technologies Conference, Sept. 25–28, Huntsville, AL. AIAA Publication 90-3666, p. 13.

CINTALA, M. J. 1992. Impact induced thermal effects in the Lunar and Martian regoliths. *J. Geophys. Res.* **97,** 947–973.

CINTALA, M. J., AND F. HÖRZ 1984. Catastrophic rupture experiments: Fragment-size analysis and energy considerations. In *Lunar and Planetary Science XV,* pp. 129–130. Lunar and Planetary Institute, Houston. [Abstracts]

DAVIS, R. D., AND E. V. RYAN 1990. On collisional disruption: Experimental results and scaling laws. *Icarus* **83,** 156–182.

FUJIWARA, A., P. CERRONI, R. D. DAVIS, E. RYAN, M. DIMARTINO, K. HOLSAPPLE, AND K. HOUSEN 1989. Experiments and scaling laws for catastrophic collisions. In *Asteroids II* (R. P. Binzel *et al.*, Eds.), pp. 240–265. Univ. of Arizona Press, Tucson.

GAULT, D. E. 1973. Displaced mass, depth, diameter, and effects of oblique trajectories for impact craters formed in dense crystalline rocks. *The Moon* **6,** 32–44.

GAULT, D. E., F. HÖRZ, AND J. B. HARTUNG 1972. Effects of microcratering on the lunar surface. *Proc. Lunar Sci. Conf. 3rd,* 2713–2734.

GAULT, D. E., AND J. A. WEDEKIND 1969. The destruction of tektites by micrometeoroid impact. *J. Geophys. Res.* **74,** 6780–6794.

GRÜN, E., H. A. ZOOK, H. FECHTIG, AND R. H. GIESE 1985. Collisional balance of the meteoritic complex. *Icarus* **62,** 244–272.

HOLSAPPLE, K. A., AND R. M. SCHMIDT 1987. Point source solutions and coupling parameters in cratering mechanics. *J. Geophys. Res.* **92,** 6350–6376.

HÖRZ, F., M. J. CINTALA, AND M. E. ZOLENSKY 1993. Hypervelocity penetration tracks in very low-density, porous targets. *Hypervelocity Impacts in Space* (J. A. M. McDonnell, Ed.), pp. 19–23. Unit for Space Sciences, University of Kent at Canterbury.

HÖRZ, F., AND R. B. SCHAAL 1981. Asteroidal agglutinate formation and implications for asteroidal surfaces. *Icarus* **46,** 337–353.

HÖRZ, F., E. SCHNEIDER, D. E. GAULT, J. B. HARTUNG, AND D. E. BROWNLEE 1975. Catastrophic rupture of lunar rocks: A Monte Carlo simulation. *The Moon* **13,** 235–258.

HOUSEN, K. R., R. M. SCHMIDT, K. A. HOLSAPPLE, AND D. R. DAVIS 1991. Scaling of fragmentation experiments conducted at elevated pressure. In *Lunar and Planetary Science XXII,* pp. 539–540. Lunar and Planetary Institute, Houston. [Abstracts]

KIEFFER, S. W. 1971. Shock metamorphism of the Coconino Sandstone at Meteor Crater, Arizona, *J. Geophys. Res.* **76,** 5449–5473.

LINDSAY, J. F. 1975. A steady-state model for the lunar soil. *Geol. Soc. Am. Bull.* **86,** 1661–1670.

MCKAY, D. S., G. HEIKEN, A. BASU, G. BLANFORD, S. SIMON, R. REEDY, B. M. FRENCH, AND J. PAPIKE 1991. The Lunar regolith. In *Lunar Sourcebook: A User's Guide to the Moon* (G. H. Heiken, D. T. Vaniman, and B. M. French, Eds.), pp. 285–356. Pergamon, Cambridge.

NAKAMURA, A., AND A. FUJIWARA 1991. Velocity distribution of fragments formed in a simulated collisional disruption. *Icarus* **92,** 132–146.

NISHIIZUMI, K., J. R. ARNOLD, D. FINK, J. KLEIN, R. MIDDLETON, D. E. BROWNLEE, AND M. MAURETTE 1991. Exposure history of individual cosmic particles. *Earth Planet. Sci. Lett.* **104,** 315–324.

POLANSKEY, C. A., AND T. J. AHRENS 1990. Impact spallation experiments: Fracture patterns and spall velocities. *Icarus* **87,** 140–155.

RUBIN, S. W., M. J. CINTALA, AND F. HÖRZ 1991. Collisional disruption experiments: Analysis of identical impacts. In *Lunar and Planetary Science XXII,* p. 1393. Lunar and Planetary Institute, Houston. [Abstracts]

STÖFFLER, D., D. E. GAULT, J. WEDEKIND, AND G. POLKOWSKI 1975. Experimental hypervelocity impact into quartz sand: Distribution and shock metamorphism of ejecta. *J. Geophys. Res.* **80,** 4062–4077.

WASSON, J. T. 1974. *Meteorites.* pp. 175–177. Springer-Verlag, New York.